Accepted Manuscript

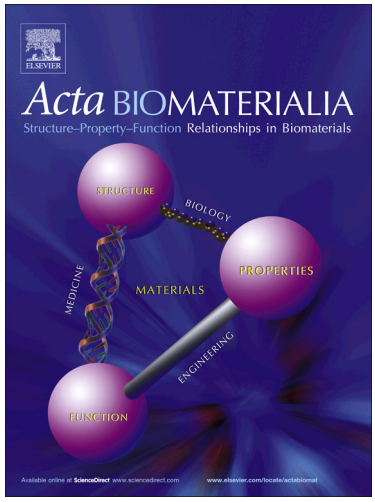

Surface Nanotopography guides Kidney-derived Stem Cells Differentiation into Podocytes

Melanie MacGregor-Ramiasa, Isabel Hopp, Akash Bachhuka, Patricia Murray, Krasimir Vasilev

PII: S1742-7061(17)30141-1
DOI: http://dx.doi.org/10.1016/j.actbio.2017.02.036
Reference: ACTBIO 4757

To appear in: *Acta Biomaterialia*

Received Date: 3 November 2016
Revised Date: 9 February 2017
Accepted Date: 17 February 2017

Please cite this article as: MacGregor-Ramiasa, M., Hopp, I., Bachhuka, A., Murray, P., Vasilev, K., Surface Nanotopography guides Kidney-derived Stem Cells Differentiation into Podocytes, *Acta Biomaterialia* (2017), doi: http://dx.doi.org/10.1016/j.actbio.2017.02.036

Surface Nanotopography guides Kidney-derived Stem Cells Differentiation into Podocytes

Melanie MacGregor-Ramiasa[a]‡, Isabel Hopp[b]‡, Akash Bachhuka[a], Patricia Murray[b] and Krasimir Vasilev[a,c]**

[a] Future Industries Institute, University of South Australia, Mawson Lakes 5095 SA, Australia

[b] Institute for Translational Medicine, University of Liverpool, Liverpool L69, United Kingdom

[c] School of Engineering, University of South Australia, Mawson Lakes 5095 SA Australia

KEYWORDS gold nanoparticle, nanotopography gradient, plasma polymers, kidney stem cell, stem cell differentiation, physical cues, nanoroughness density, podocytes, proximal tubule cells.

ABSTRACT Stem cells have enormous potential for developing novel therapies for kidney disease but our current inability to direct their differentiation to specialised renal cells presents a barrier to their use in renal bioengineering and drug development programmes. Here, a plasma-based technology was used to produce a range of biocompatible substrates comprising controlled surface nanotopography and tailored outermost chemical functionalities. These novel substrata were used to investigate the response of mouse kidney-derived stem cells to changes in both substrate nanotopography and surface chemistry. The stem cells proliferated to a similar extent on all substrates, but specific combinations of nanotopography and surface chemistry promoted differentiation into either podocyte or proximal tubule-like cells. The data reveal that high density of surface nanodefects in association with amine rich chemistry primarily lead to differentiation into podocytes while surfaces with low amine content constituted better substrates

for differentiation into proximal tubule cells regardless of the surface nanotopographic profile. Thus plasma coated nanorough substrate may provide useful platform for guiding the fate kidney stem cell in vitro.

1- Introduction

Chronic kidney disease (CKD) is a global epidemic for which very limited treatment options are available. To date, the only two alternatives available to patients with end stage renal failure are dialysis or kidney transplantation. Transplantation is the gold-standard treatment but there is a shortage of donors. Dialysis is economically very costly and is associated with high rates of morbidity and mortality and poor patient quality of life.[1] Stem cell-based therapies are emerging as a potent new approach to address this public health issue [2, 3] and have been found to be therapeutic in various rodent models of kidney disease.[4, 5] Stem cells also have potential in renal bioengineering, for understanding disease mechanisms[6] and in drug development programmes,[7] but for these applications it is necessary to direct the differentiation of the cells to specialised renal cell types. Stem cell-derived podocytes and proximal tubule cells (PTCs) are of particular interest for drug development because these cell types are implicated in the most common types of CKD, including diabetic nephropathy.[8, 9] However, progress in this field is limited by the lack of appropriate in vitro culture systems for promoting growth and controlling differentiation.[10, 11] Our previous work has shown that mouse kidney-derived stem cells (mKSCs) can spontaneously generate renal-specific cell types, such as PTCs and podocytes during in vitro culture, but differentiation was poorly controlled, so that only a sub-set of the population differentiated to the required cell type.[12, 13]

It is well accepted that soluble factors, such as growth factors and cytokines, are critical in regulating the fate of stem cells. Besides soluble cues, however, the material properties of the

underlying substrate also play a crucial role in directing stem cell adhesion, growth, and eventually their differentiation.[14-17] Since no in vitro nor any in vivo cell culture substrate is molecularly smooth, the effect of surface topography on cell fate is of particular interest [18-20], with the important role of nanoscale features becoming increasingly apparent.[15, 21] Indeed, recent studies have demonstrated that surface nanotopography affects the adhesion and growth of various cell lines [22] and can influence stem cell differentiation.[23, 24] This is likely due to the fact that nanotopographical features can induce changes in the structure of the cellular cytoskeleton, [15, 25] thus triggering mechano-transduction events that can cause changes in gene expression, which ultimately lead to differentiation.[14, 26, 27]

Nevertheless, based on our current understanding of these molecular mechanisms, it is not possible to predict the effect that nanotopography will have on any specific cell type. In previous work, we used plasma polymer gradients of surface chemistry as high-throughput vectors for screening the behaviour of mouse embryonic stem cells.[28, 29] Cell-surface interactions, such as adhesion and spreading, varied with surface chemistry and this strongly affected phenotype, with stemness being better maintained on surfaces that favoured the formation of multi-layered colonies rather than monolayers.[30] These studies clearly demonstrated that cell surface interactions dictate stem cell differentiation.

We have recently shown that surface chemistry is an important parameter that influences the differentiation of mKSCs into specialised renal cell lines. We used Allylamine (AA) and Octadiene (OD) composed homo- and co-polymeric plasma coatings and found that AA-rich surfaces promoted cell differentiation into podocytes whereas OD richer surfaces directed differentiation into PTCs.[7] Here, in order to assist the development of culture systems that are able to promote the differentiation of mKSCs to specific linages, we have used plasma

deposition methods to produce a library of substrates with increasing nanoroughness in combination with specific surface chemistries.[31] This technique has the advantage of being highly reproducible and environmentally friendly, in the sense that it does not require the use of organic solvents. Furthermore, plasma deposition is easily scalable and can be used to modify the chemistry, wettability, topography and adhesion properties of any material.[32] For these reasons, plasma deposition has become a tool of choice for the production of novel functional biomaterials.[33] We show here that mKSCs are sensitive to both chemical and topographical variation, and that specific combinations of nanotopography and surface chemistry can promote the differentiation of mKSCs to either podocytes or PTCs.

2- Experimental section

2-1. Gold nanoparticle synthesis. Gold nanoparticles (AuNPs) were synthesized by reducing hydrogen tetrachloroaurate ($HAuCl_4$, 99.9985%, ProSciTech) with trisodium citrate (TSC, 99%, BHD Chemicals, Australia Pty. Ltd.) as per Zhu et al. method.[34] Briefly, a 1% TSC solution was added to 50 mL of boiling $HAuCl_4$ solution (0.01 %) under vigorous stirring.[35] The amount of reacting TSC determines the size of the AuNPs. 1 mL and 0.3 mL of TSC were added in order to produce particles with 16 nm and 68 nm diameter, respectively. The solution was kept under the boil for another 20 minutes period over which the color of the reaction solution changes from light yellow to deep red. Once the color change was complete the solution was allowed to cool to ambient temperature. In order to modify the surface of the AuNPs, a large excess of 2-mercaprosuccinic acid (MSA, 97%, Aldrich) was subsequently added to the AuNPs solution. A 10^{-2} M Na_2(MSA) solution was prepared by stoichiometric neutralisation of the thiol with sodium hydroxide. 7.5 mL of the Na_2(MSA) solution were added to the prepared AuNPs

suspension, and left to react overnight at 50°C under constant stirring. The nanoparticles suspension were kept in the dark at 4°C until further use.

2-2. Plasma polymer substrates Plasma polymerization was carried out in a custom-built 13.56 MHz radiofrequency plasma reactor described previously.[36] 13 mm tissue culture treated thermanox coverslips were introduced in the chamber and cleaned by applying a 3 minutes air plasma. On all substrates, except the tissue culture plate control, an allylamine under layer (AA) (98%, Aldrich) was first deposited at a flow rate of 10 standard cubic centimetres per minute (sccm) for 3 minutes. The purpose of the resulting plasma deposited polyallylamine films (ppAA) is to facilitate the surface immobilisation of the AuNPs, as described below. Following the nanoparticles adsorption, 5 nm thick overcoatings were deposited on the nanorough substrates in order to control their outermost chemistry. Allylamine and 1,7-octadiene (98%, Aldrich) precursor were mounted on two separate needle valves. In order to achieve different overcoatings surface chemistry, the ratio of allylamine and octadiene allowed to enter the plasma chamber was carefully controlled by the automated needle valves. Composition of monomers used consisted of 100% AA; 75%AA/25%OD; 25%AA/75%OD and 100%OD. In the following these coating are referred to as 100%AA, 75%AA, 25%AA and 0%AA. In all cases the total precursor flow rate was 10 sccm, and the plasma polymer films were deposited for 30 seconds at 30 W.

2-3. Preparation of nanorough substrates. Homogeneous nanorough substrates were prepared by immersing the substrates coated with the ppAA underlayer in AuNPs solution for 2 and 6h, for the 16 and 68 nm particles, respectively. In this way, electrostatic interaction between positively charged surface amine groups and negatively charged nanoparticles drive the binding of the nanoparticles to the substrates. Nanoroughness gradient substrates were prepared by

gradually adsorbing the nanoparticles onto the ppAA coated coverslips. The immersion time was controlled by progressively dipping the substrates in the AuNPs solution using a linear motion drive dip coater (Zaber T-LSR series)[37]. The rate of immersion was 5 mm/h and 1.66 mm/h for the 16 and 68 nm AuNPs, respectively. Once 10 mm of the substrate had been immersed, the substrates were promptly withdrawn from the solution and thoroughly rinsed with MilliQ water in order to wash off loosely bound particles. This way, the section of the gradient samples that were in the AuNPs solution for the longest time, were immersed for 2 and 6h for 16 and 68 nm particles respectively, just like the corresponding homogeneous samples. For the substrates physico-chemical analysis and cell culture assays, the gradient samples were divided into 5, 2mm wide sections along the axis of increasing nanoparticle coverage, as sketched in Figure 1.a.

2-4. Atomic force microscopy. An NT-MDT NTEGRA SPM atomic force microscope (AFM) was used in non-contact mode to provide topographical images. Silicon nitride non-contact tips coated with gold on the reflective side (NT-MDT, NSG03) and with resonance frequencies between 65 and 100 kHz were used. The amplitude of oscillation was 10 nm, and the scan rate for 5 μm x 5 μm images was 0.5 Hz. The scanner used had a maximum range of 100 μm and was calibrated using 1.5 μm standard grids with a height of 22 nm.

2-5. X-ray photoelectron spectroscopy (XPS). XPS analysis was used to determine the surface composition of the plasma polymer and the gradients of deposited AuNPs. XPS spectra were recorded on a Specs SAGE XPS spectrometer using Al Kα radiation source (hν = 1253.6 eV) operated at 10 kV and 20 mA. Elements present in a sample surface were identified from the survey spectrum recorded over the energy range 0–1000 eV at a pass energy of 100 eV and a resolution of 0.5 eV. The areas under selected photoelectron peaks in a widescan spectrum were used to calculate percentage atomic concentrations (excluding hydrogen). All the binding

energies (BEs) were referenced to the C1s neutral carbon peak at 285 eV, to compensate for the effect of surface charging. The XPS analysis area was circular with a diameter of 0.7 mm. The processing and curve-fitting of the high-energy resolution spectra were performed using CasaXPS software.

2-6. Cell culture and analyses. mKSCs [12] were cultured in high glucose DMEM (Sigma) supplemented with 2 mM L-glutamine (Sigma), 1% non-essential amino acids (Life Technologies) and 10% FBS (Sigma). Cells were cultured in a humidified chamber in an atmosphere of 5% CO_2 at 37 °C. Cells were cultured for 96 h on the novel substrates and medium was changed every second day. All experiments were carried out using cells between passage 15 and 25. The mKSCs used in this study were isolated from a single neonatal mouse kidney and a clonal cell line was identified that was able to differentiate into a range of kidney-specific cell types, including proximal tubule-like cells that display megalin-dependent absorptive functions. [12] In addition, mKSCs were able to generate PTCs and podocytes that were located within developing nephrons using a chimeric kidney rudiment culture system.[12, 13] A thorough characterisation of these cells can be found in the literature. [12, 13]

2-7. Live cell imaging and podocyte identification. For mKSC and podocyte-like cell quantification, $1x10^3$ cells/well were seeded into 24 well plates (Corning®) in 500 µL of cell culture medium. Cell numbers were determined 24 and 96 h post seeding from phase contrast images obtained during live cell imaging (CellIQ, Chip-man Technologies) from 10 different areas across homogeneously coated samples as well as 5 per section across gradients substrates. For the gradient substrates, the 5 imaging subdivisions corresponded to the areas 1 to 5 defined in the above substrate characterisation section and illustrated in Figure 1.a. Podocytes were identified from characteristic morphological features, which included high cytoplasmic-to-

nuclear ratio, arborized appearance and a high incidence of binucleation and counted by eye following established procedures.[12, 13, 38] A minimum of 10 images per coverslip and a total number 80 cells per field of view was analysed. The number of podocyte-like cells was then quantified relative to cells that did not show podocyte characteristic features. All experiments were performed in 3 biological replicates.

2-8. Immunostaining. Cultured cells were fixed in 4% paraformaldehyde (PFA) for 5 minutes at room temperature and washed with PBS. The following primary antibodies were used: anti-Wt1 (1:100, Millipore, 05-753), anti-nephrin (1:500, Abcam, ab58968) and anti-megalin (1:200, Acris, DM3613P). The secondary antibodies were Alexa fluor-conjugates (1:500) (Life Technologies). F-actin was stained using Alexa flour conjugated phalloidin (1:250, Thermo Fischer). Nuclei were stained with DAPI (Life Technologies). Images were collected using a Leica DFC350FX camera connected to a Leica DM2500 fluorescence microscope.

2-9. Cell count and PDT: Cultured cells were fixed in 4% paraformaldehyde (PFA) for 5 minutes at room temperature and washed with PBS. Subsequently nuclei were stained with DAPI (Life Technologies) and a minimum of 10 images were taken per coverslip using a Leica DFC350FX camera connected to a Leica DM2500 fluorescence microscope. Cell number was then quantified by counting the number of nuclei per image using ImageJ software.[39] Population doubling time (PDT) was then determined from these cell numbers by employing nonlinear regression analysis using the following equation: $PDT = \ln(2)/K$ where K is the rate constant.

2-10. Statistical Analysis: Standard deviation (SD) error was used for descriptive analysis and standard error of the mean (SEM) for inferential statistics with a minimum of 3 independently conducted experiments (n=3). One-way analyses of variance (ANOVA) and post-hoc Tukey test were performed to evaluate statistical significances between two groups of samples. All

statistical analyses were performed using Graphpad (GraphPad Prism v5.0 software for Windows, GraphPad Software Inc., San Diego, CA). The statistical significance is shown using the *p*-value (*p*), which was considered "significant" with $p<0.05$ (*); "very significant" with $0.01>p>0.001$ (**) and "very highly significant" with $p<0.001$ (***).If no significant difference was detected between data sets this is indicated either in the figure captions or indicated by n.s. (not significant) within the graphs.

3- Results

3-1. Substrate physico-chemical characterisation. The influence of surface nanotopography on the fate of mKSCs was determined by assessing cells growth and differentiation on nanoengineered substrates where gold nanoparticles (AuNPs) were used to generate controlled surface naotopography. Two differently sized nanoparticles, 16 nm and 68 nm in diameter, were used to generate substrates with both uniform nanoparticle surface density and as nanoparticles number density gradients (Figure 1a). Representative AFM images of the 16 nm and 68 nm gradient substrata are shown in Figure 1b and c, respectively. The surface bound AuNPs are nearly monodispersed in size and not aggregated. For both sizes, the AuNPs density increases as a function of the position on the gradient, 1 to 5 (Figure 1a). As a consequence, both the surface area and root mean square (RMS) roughness of the substrates increases over the length of the gradient, as shown in Figure 1d and e, respectively. The AuNPs surface density on the homogeneous nanorough substrates correspond for both 16 and 68 nm particles to that of position 5 on the gradients.

In addition to the different topographies, 4 distinct surface chemistries were generated by plasma polymer co-deposition of allylamine and octadiene precursors in different proportions.

Namely the controlled overcoating consisted of plasma deposited copolymer containing 100% allylamine (100% AA); 75% allylamine-25% octadiene (75% AA), 25% allylamine-75% octadiene (25% AA) and 100% octadiene (0% AA) (Figure 1. A, right). Typical carbon to nitrogen ratio and gold atomic content for the 68 and 16 nm gradients sample sets are shown in Figure 2a and b, respectively. The atomic content, determined from XPS survey spectra for the entire set of samples used in this study is provided in Supporting Information, Table 1. Substrates contain carbon, nitrogen and oxygen species in good agreement with previous studies. [28, 40-42] Compared to uncoated gradient substrates, the nitrogen atomic content increases as the proportion of allylamine used for the polymer deposition increases. Across the gradient, the C/N ratio is essentially constant for a given overcoating chemistry, thus indicating that the plasma deposited thin films indeed provide a uniform surface chemistry over the topographical features. It is worth noting that since 100% AA coating was used for the electrostatic binding of the AuNPs onto the substrates, the uncoated gradients also contain nitrogen, but in lesser amounts than the 100% AA overcoating due to the presence of uncoated gold nanoparticles. The plasma deposition conditions were chosen so as to ensure the deposited polymeric films were continuous and pinhole free (thickness > 5 nm), and yet did not shield the underlying nanotopography as per previously published work [37, 43] The presence of gold in the XPS survey spectra indicates that the plasma polymer overcoating layer is thinner than 10 nm in thickness, which is suitable for retaining the underlying topographic profile.[37] Finally, the gold atomic content increases over the length of the gradient.

3-2. Cell proliferation. The response of mKSCs to surface nanotopography and chemistry was probed by analysing cell attachment and proliferation on the substrates. Firstly, cells were seeded on substrates with a uniform distribution of AuNPs across the surface, coated with 16 nm or 68

nm AuNPs that were overcoated with thin plasma films composed of 100% AA, 75% AA, 25% AA or 0% AA. The cells adhered to and proliferated on all substrates. The cell density, as recorded after 24 and 96 h in culture, is comparable for all substrates investigated. Population doubling time (PDT) analysis showed that mKSCs require about 26 ± 2 h to double their population on all substrates. The data demonstrate that none of the substrates significantly inhibit or enhance cell proliferation.

Cell proliferation was subsequently assessed on the nanotopography density gradients. The change in cell number across the nanotopography gradient 24 and 96 h post seeding is provided in supplementary information Figure S2 for both AuNPs sizes and the 4 distinct surface chemistries. At 24 h, cell numbers were higher on the 68 nm substrates, but by 96 h the cells had proliferated similarly on all substrates and displayed equal cell density across the gradients, regardless of AuNPs size and plasma coating. Similarly, we did not find significant differences in PDT ($p > 0.05$) (Figure S3).

3-3. Cell differentiation. Previous studies have shown that mKSCs can spontaneously differentiate into podocyte- and proximal tubule-like cells in the presence of soluble cues within the cell culture medium.[12] Here we interrogate for the first time the combined effect of substrate nanotopography and surface chemistry on mKSC differentiation.

3-3.1 Differentiation of mKSCs into podocytes. To investigate whether mKSCs differentiate into podocytes in response to surface chemistry and nanotopography, the number of podocyte-like cells was quantified 96 h post seeding. Podocyte differentiation was first investigated on samples with homogeneous surface nanotopography but different chemistries. Podocyte-like cells were identified by their typical morphological features that include high cytoplasmic-to-nuclear ratio, arborized appearance and binuclearity as described previously.[12, 44] The quantification of

podocyte-like cells on the 16 and 68 nm substrates are presented in Figure 4 for all 4 surface chemistries. By 96 h post seeding, it was found that the number of podocyte-like cells on the homogeneous nanorough substrates increased with increasing AA content. Nanotopography size did not seem to affect the number of cells differentiating into podocytes. Although there were slightly larger numbers of podocyte-like cells on the surfaces containing 68 nm nanotopography, these differences were not statistically significant.

Podocyte differentiation was then interrogated in the same way on nanotopography gradient substrates (Figure 5). The results confirm the above findings, where there is an increase in podocyte-like cell number with increasing AA surface content. Moreover, the proportion of podocyte like-cells increases with increasing AuNPs density across the gradient. This trend is consistent, regardless of the AuNPs size and plasma overcoating chemistry. The percentages of podocyte-like cells is overall highest on AA rich coatings with high AuNPs density (35%), and lowest on substrates comprising 0% AA with low AuNPs density (10-15%). Our data therefore show that the optimal surface properties for initiating podocyte differentiation are high nitrogen (amine) concentration and high nanoroughness density.

Subsequently, mKSCs were immunostained to examine the presence of two specific podocyte markers, WT1 and nephrin, 96 h post seeding. Figure 6 shows representative images of cells cultured on 16 nm AuNPs density gradients coated with either AA rich or OD rich plasma film. The results show that both markers are expressed in cells that were cultured on amine rich coatings. The expression of the podocyte markers increases along the nanotopography gradient, in good agreement with the percentage of podocyte-like cells calculated and presented in Figure 5. Images for the rest of the experimental conditions are provided in the Supporting information.

3-3.2 Differentiation of mKSCs into proximal tubule cells. The substrates were also assessed for their influence on PTC differentiation. PTCs express megalin, which is responsible for the endocytic uptake of albumin from the glomerular filtrate. In Figure 7 representative images show mKSCs stained for megalin (green) across the 16 nm and 68 nm nanotopography density gradient overcoated with either a OD or AA rich plasma coating. Typical images for the whole range of experimental conditions are provided in supporting information. The results show that AuNPs surface density does not appear to influence megalin expression. However, more cells appeared to express megalin on the octadiene-rich substrates (0%AA).

4- Discussion

While many reports in the literature demonstrate that together both surface nanotopography and chemistry contribute to changes in the fate of stem cells, interrogating the individual effect of these two type of environmental cues is still challenging.[45] Here, in order to isolate the specific contribution of mechanical cues from other surface chemistry related signals in modulating mKSC differentiation towards different kidney cell lineages, we developed a plasma based approach to generate specially designed nanorough substrates. We produced a range of biocompatible substrates comprising nanoengineered topography gradients with tailored outermost surface chemistries. Using this experimental method we were able to compare the effect of surfaces which had the same outter chemistry but different nanoroughness (and vice-versa), on the differentiation of mKSC. ~~These novel substrates were used to investigate both the individual and combinatory effect of surface nanotopography and chemistry related cues in modulating mKSC differentiation towards podocytes or proximal tubule cells phenotype.In this study, we produced a range of biocompatible substrates comprising nanoengineered topography gradients with tailored outermost surface chemistries. These novel substrates were used to~~

~~investigate the combinatory effect of surface nanotopography and chemistry on the behaviour of mKSCs.~~ The key finding was that surfaces with the highest surface density of AuNPs and highest AA content promoted podocyte differentiation. PTC differentiation was not affected by the degree of surface roughness, controlled by the surface AuNPs density, but in contrast, podocyte differentiation appeared to be stimulated on surfaces with lowest AA content.

Plasma facilitated methods well establish in our laboratory [37, 46-48] were used to produce substrates with either uniform coverage or number density gradient distribution of near monodisperse gold nanoparticles 16 or 68 nm in diameter. As a result, in the set of model substrates used in this study, the vertical and lateral dimensions of the nanofeatures were varied as well as the overall surface area (Figure 1). The RMS roughness of the substrate increases over the gradient substrates from 3 to 6 nm for the 16 nm AuNPs, and from 7 to 16 nm for the larger 68 nm AuNPs. The surface area increases by a maximum of 10% for the small nanoparticles, but up to 42% for the large ones. Additionally, all substrates were coated with a nanothin (5 nm) organic plasma polymer film of desired chemical composition. Therefore, the outer surface chemistry on the gradients was uniform (Figure 2a) while the nanotopography of the substrates was preserved (Figure 2b). Owing to this careful substrate design, we were able to decouple the effect of topography and chemistry. On any given gradient substrate, it was possible to explore the effect on the mKSC of surface cues which were uniquely topographical in nature, through gradual changes in the density of the physical features along one axis. Nanotopography gradients with controlled chemistry are in this way a powerful means to elucidate the effect of the extracellular matrix physical properties on cell behaviour by providing contact guidance cues. It is worth noting here that the gold nanoparticles used in this study to impart nanoroughness to the growth substrate, were selected because they are chemically inert, in the size range used, and

therefore do not cause adverse cellular reaction. Besides, the thin but pinhole-free plasma polymer coating deposited on top of the gold nanoparticles prevents them from entering in direct contact with the cells. Furthermore, the gold nanoparticles are strongly bound to the substrates via electrostatic interaction and are therefore highly unlikely to penetrate the cells. Under the experimental conditions investigated, no nanotoxicity was observed.

While we have shown in our previous work that AA and OD composed plasma polymers allow cell attachment and proliferation,[22, 28] here we explored the additional effect of nanotopography on cell behaviour. The presence of nanosized topographical features in the natural extracellular matrix has been reported [49, 50] and it is now believed that only nanostructures of size similar to those of natural proteins affect their potential denaturation [51] which in turn would dictate the fate of cells. For this reason we choose two different nanoparticle sizes 16 and 68 nm, which correspond to the size of an individual medium-size protein such as laminin, and a small protein cluster, respectively.[52] Previous studies have shown that various cell types are indeed sensitive to minute changes in nanofeatures scale and that they may react differently to nanosized physical cues. For instance, published studies have shown that human mesenchymal stem cells, rat osteoblast and rat fibroblasts had a higher proliferation rate on surfaces with 200 nm features (opposed to 1500 or 50 nm),[53] whereas the proliferation rate of human embryonic kidney cells (HEK-293) was higher on surfaces with 40 nm features than 100 nm ones.[54] Other studies exploring the effect of nanofeatures surface density on primary fibroblasts highlighted that cell adhesion and spreading decreased as a function of nanoparticle size and was optimal for 16 nm particles with densities between 50 and 140 np/um2.[22] The only regions of the gradients investigated in the present work with corresponding nanoparticle densities are section 2 to 5 on the 16 nm substrate (Figure 8.a). However, in this work we found

that mKSC attachment and proliferation was not significantly affected by nanotopography, as all substrates supported cell attachment and proliferation to a similar degree regardless of AuNPs size, density and plasma coating chemistry (Figure 3, Figure S2 and S3).

mKSC behaviour was not affected by AuNPs size. However, differentiation to podocyte-like cells was significantly enhanced by increasing the amount of AA on the surface (e.g., the mKSC population comprised 10% podocytes on 0% AA, and 20% on 100% AA), thus indicating that substrate chemistry strongly influences mKSC differentiation. Amine rich surface coatings are known for their good biocompatibility and previous studies have demonstrated that such surfaces can enhance the differentiation of stem cells.[7, 28, 55] The unique properties of amine rich substrates derive from their propensity to bind proteins. In physiological conditions, the localised positive charge of protonated amine groups engage with negatively charged biomolecules, such as the extracellular matrix (ECM) proteins, fibronectin and vitronectin that are present in serum. Depending on how they are presented by the plasma-functionalised substrates, these ECM proteins could then serve as a reservoir for important signalling molecules such as FGFs, BMPs and Wnts, and also engage cell membrane receptors, such as integrins, thereby initiating complex molecular mechanisms which can regulate proliferation and differentiation. For instance, it has been shown that engagement of integrin β1 can regulate the differentiation and maintenance of podocytes.[56]

Using nanoparticle density gradients, we further demonstrated that podocyte differentiation depended on nanofeatures number density and was greater on the denser part of the nanotopography gradients, where the podocyte component of the population reached ~35%. Surface nanotopography may trigger podocyte differentiation via 2 different mechanisms. Firstly, the increase in nanoparticle density is accompanied by an increase in surface area (Figure

1d) and so more protein could theoretically adsorb onto the surface. Moreover, the nanotopographical landscape of the nanorough substrate may lead to a diversity in protein orientation and so increase or reduce their bio-availability. This enhanced protein adsorption could promote the differentiation of mKSCs into podocytes, especially if the surface bound proteins were bioactive and similar to those present in the glomerular basement membrane, which is the natural ECM of podocytes. It is indeed well accepted that substrates mimicking natural ECMs promote differentiation. [57] Secondly, the nanofeatures could be directly acting on the cytoplasmic membrane of the mKSCs and trigger differentiation by mechanical action. Previous studies have, for instance, shown that neuronal [58-60] and myogenic [27, 61] differentiation can be triggered by surface nanofeatures. Interestingly, neurones and myoblasts, share some morphological features with podocytes in that they also have relatively large cytoplasm and elongated protuberances. Our findings, together with those of previous studies [27, 58-61] indicate that differentiation into large cells with defined cytoplasmic features are particularly stimulated by discrete surface nanotopography, such as pits, nanofibers or, here, nanoparticles.

It is worth noting, however, that the increase in nanoparticle density was associated with an increase in podocyte –like cells, regardless of the nanoparticles diameter and surface chemistry. In all cases, we detected significantly more cells towards rougher regions of the gradient. The percentage of podocyte like-cells is presented in Figure 8b as a function of the AuNPs number density for both nanoparticle size combined. The percentage of podocyte-like-cells increases logarithmically with the number of AuNPs/ μm^2, irrespective of AuNPs size. In contrast, the number of podocyte like cells doesn't directly correlate to the actual surface area (Figure 8c). This result suggests that out of the two mechanism proposed above, the mechanical action of

surface nanocues may have a greater impact on podocyte differentiation than an increase in surface area associated with enhanced protein absorption. Our results demonstrated that podocyte differentiation is independently promoted by 1) increasing number density of surface nanofeatures and 2) amine rich chemistry. Furthermore, our results show that these effect are additive as combining both favourable physical and chemical cues results in the greatest amount of podocyte differentiation.

In contrast to podocyte differentiation, which was higher on AA-rich substrates, PTC differentiation appeared to be enhanced by culture on the octadiene-rich substrates (i.e., low AA). This is perhaps not too surprising because evidence suggests that the concentration of certain signalling molecules, especially Wnts, can influence whether nephron progenitor cells in the developing embryo kidney adopt a podocyte or PTC fate.[62] For instance, it has been suggested that high levels of Wnts trigger PTC differentiation and inhibit podocyte differentiation, whereas lower levels of Wnts are associated with podocyte differentiation.[62] Thus, it would be expected that culture conditions designed to promote podocyte differentiation would show a corresponding reduction in the extent of PTC differentiation.

5- Conclusions

In summary, substrates displaying controlled nanotopographical features and finely tailored outermost surface chemistry were produced via gold nanoparticle surface immobilisation and subsequent plasma polymer deposition. This approach allowed us to decouple the role of topography and other surface chemistry related cues in modulating the fate of mKSC. Thorough AFM and XPS surface characterisation established the differences in surface chemistry and nanoroughness between the substrates prepared with nanoparticles 16 and 68 nm in diameter. ~~were used to investigate the fate of mKSCs.~~ All these model surfaces, with either homogeneous

or gradient nanotopography, supported cell adhesion and proliferation. Neither AuNPs size nor density had significant effects on cell proliferation, whereas mKSC differentiation into podocytes and PTCs was highly dependent on surface chemistry. Amine rich surface chemistry promoted mKSC differentiation into podocytes while substrates coated with octadiene provided a better platform for differentiation into proximal tubule-like compared to alyllamine-rich surfaces. Furthermore, culturing mKSCs on nanotopography density gradients demonstrated that podocyte differentiation was enhanced on rougher surfaces with high nanofeature density while PTC differentiation was independent of surface topography. Our result indicates that, although the type of surface nanotopography investigated here does not seem to affect mKSC adhesion and proliferation significantly, it certainly influences their differentiation. This works also proves that plasma-based methods can be used to control both surface nanoroughness and chemistry in order to prepare growth substrate capable to direct mKSC differentiation towards either PTC or podocytes. Our results further suggest that a simple increase in surface area may not be a factor as determining of the cell fate as the actual number of surface nanodefect. These findings raise questions on the role of individual physical cues on the mechanism of mKSC differentiation into podocytes which requires further investigations.

SUPPLEMENTARY MATERIAL

XPS atomic content for the full range of substrates. WT1, nephrin and megalin immunostaining micrograph for all gradient substrates.

AUTHOR INFORMATION

Corresponding Author

* K. Vasilev email: krasimir.vasilev@unisa.edu.au

* P. Murray email: P.A.Murray@liverpool.ac.uk

AUTHOR CONTRIBUTIONS

The manuscript was written through contributions of all authors. All authors have given approval to the final version of the manuscript. ‡MMR and IH contributed equally.

FUNDING SOURCES

Australian Research Council Discovery Project DP15104212

University of South Australia Research Theme Investment Scheme 2015

Channel 7 Children Research Foundation (Project 15976)

The South Australian state Government Premier Research and Industry Fund

The Humboldt Foundation for Humboldt Fellowship for Experienced Researchers

EU FP7 Initial Training Network, 'NephroTools'.

NHMRC for Fellowship APP1122825

ACKNOWLEDGMENT

The work was partially supported by ARC DP15104212. The authors also acknowledge funding from the University of South Australia Research Theme Investment Scheme 2015, Channel 7 Children Research Foundation (Project 15976), the South Australian state Government Premier Research and Industry Fund and EU FP7 Initial Training Network, 'NephroTools'. MMR also acknowledge the support provided by the UniSA ECR networking award. KV also thanks NHMRC for Fellowship APP1122825 and the Humboldt Foundation for the Humboldt Fellowship for Experienced Researchers.

455 FIGURE CAPTIONS

456 **Figure 1:** Quantitative analysis of nanoparticle gradients. **a.** Schematic of the gradient substrates
457 investigated identifying on the left the gradient sections 1 to 5 with increasing number of surface
458 bound AuNPs and on the right, the 4 different surface chemistry investigated 0%AA, 25%AA,
459 75%AA and 100%AA. **b.** and **c.** 5x5µm AFM images of the 16 nm and 68nm nanoparticle
460 gradient, respectively, for position 1 to 5 across the gradient. Images were recorded every 2 mm
461 across the gradient from 2 mm (position 1) to 10 mm (position 5). The scale bar corresponds to
462 1µm. **d.** percentage of increased surface area and **e.** RMS roughness in nm across the gradients
463 for both sizes of nanoparticles.

464 **Figure 2:** XPS atomic concentration analysis. Elements were identified from survey spectra. All
465 binding energies were referenced to the C1s neutral carbon. **a.** Ratio of carbon to nitrogen (C/N
466 ratio) on the 68nm gradient and **b.** gold atomic concentration, in %, on the 16nm gradient both
467 measured at 5 positions across the gradient with 1 being the lowest and 5 being the highest
468 AuNPs density.

469 **Figure 3**: **a.** and **b.** Cell proliferation. **c.** and **d.** Cell population doubling time (PDT) of mKSCs
470 seeded on substrates with homogeneous AuNPs coating, 16 nm (**a.** and **c.**) and 68 nm (**b.** and **d.**)
471 in size. The cells were seeded at a density of $1x10^3$ cells per well and cultured for a period of 96
472 h. Bare tissue culture treated substrates (Tx) and 100% AA control (w/o AuNPs) were used as
473 controls. Data represent an average of 3 biological replicates. Error bars represent SEM. No
474 statistical differences were found ($p>0.05$).

475 **Figure 4**: Quantification of podocyte-like cells on substrates with homogeneous
476 nanotopography. The cells were seeded at a density of $1x10^3$ cells per well and the number of

podocyte-like cells was determined 96 h post seeding. Data represent an average of 3 biological replicates. Error bars represent SEM and asterisks indicate statistical significance compared to the 100% AA coated equivalent ($p<0.0001$).

Figure 5: Quantification of podocyte-like cells on substrates that display AuNPs density gradients overcoated with plasma films 96 h post seeding **a.** 16 nm AuNPs and **b.** 68 nm AuNPs. A bare tissue culture treated (Tx) substrate was used as control. The cells were seeded at a density of $1x10^3$ cells / well containing a 13 mm coated coverslip. Data represent an average of 3 biological replicates. Error bars represent SEM and asterisks indicate statistical difference compared to an untreated Tx control ($p<0.0001$). No significant difference between 16 nm and 68 nm AuNPs was detected ($p>0.05$).

Figure 6: Immunofluorescence images of mKSCs stained for podocyte markers across 16nm AuNPs density gradients. **a.** WT1 (green) co-stained with phalloidin to label F-actin (red) **b.** Nephrin (red) counterstained with DAPI nuclear stain (blue). In both cases, the cells were seeded at a density of $1x10^3$ cells per well and cultured for 96 h. Scale bars correspond to 100 μm.

Figure 7: Megalin staining. Immunofluorescence images of mKSCs stained for the PTC marker megalin (red) and co-stained with DAPI (blue) across the **a.** 16 nm and **b.** 68 nm AuNPs density gradient. Cells were seeded at a density of $1x10^3$ cells per well and cultured for 96 h. Scale bars correspond to 100 μm.

Figure 8. a. Number of AuNPs per unit area for both Np sizes. **b.** Number of podocyte-like cells in % as a function of AuNPs density for 16 and 68 nm combined. The solid lines correspond to a 2 parameter logarithm function fit. The r^2 values are 0.73, 0.75, 0.69 and 0.78 for 100%,

75%,25% and 0%AA respectively. **c.** Number of podocyte-like cells in % as a function of the actual surface area.

REFERENCES

[1] Trivedi H. Cost implications of caring for chronic kidney disease: are interventions cost-effective? Adv Chronic Kidney Dis 2010;17:265-70.
[2] Pleniceanu O, Harari-Steinberg O, Dekel B. Concise review: Kidney stem/progenitor cells: differentiate, sort out, or reprogram? Stem Cells 2010;28:1649-60.
[3] Hopkins C, Li J, Rae F, Little MH. Stem cell options for kidney disease. J Pathol 2009;217:265-81.
[4] Murray PA, Woolf AS. Using stem and progenitor cells to recapitulate kidney development and restore renal function. Current Opinion in Organ Transplantation 2014;19:140-4.
[5] Sharkey J, Scarfe L, Santeramo I, Garcia-Finana M, Park BK, Poptani H, Wilm B, Taylor A, Murray P. Imaging technologies for monitoring the safety, efficacy and mechanisms of action of cell-based regenerative medicine therapies in models of kidney disease. European Journal of Pharmacology 2016.
[6] Wilm B, Tamburrini R, Orlando G, Murray P. Autologous Cells for Kidney Bioengineering. Current Transplantation Reports 2016:1-14.
[7] Murray P, Vasilev K, Fuente Mora C, Ranghini E, Tensaout H, Rak-Raszewska A, Wilm B, Edgar D, Short RD, Kenny SE. The potential of small chemical functional groups for directing the differentiation of kidney stem cells. Biochem Soc Trans 2010;38:1062-6.
[8] Yoo T, Li J, Kim J, Jung D, Kwak S, Ryu D, Choi H, Kim J, Kim H, Han S. Activation of the renin–angiotensin system within podocytes in diabetes. Kidney Int 2007;71:1019-27.
[9] Magri CJ, Fava S. The role of tubular injury in diabetic nephropathy. Eur J Intern Med 2009;20:551-5.
[10] Lutolf MP, Gilbert PM, Blau HM. Designing materials to direct stem-cell fate. Nature 2009;462:433-41.
[11] Takasato M, Er PX, Becroft M, Vanslambrouck JM, Stanley EG, Elefanty AG, Little MH. Directing human embryonic stem cell differentiation towards a renal lineage generates a self-organizing kidney. Nat Cell Biol 2014;16:118-26.
[12] Fuente Mora C, Ranghini E, Bruno S, Bussolati B, Camussi G, Wilm B, Edgar D, Kenny SE, Murray P. Differentiation of podocyte and proximal tubule-like cells from a mouse kidney-derived stem cell line. Stem cells and development 2012;21:296-307.
[13] Ranghini E, Mora CF, Edgar D, Kenny SE, Murray P, Wilm B. Stem Cells Derived from Neonatal Mouse Kidney Generate Functional Proximal Tubule-Like Cells and Integrate into Developing Nephrons <italic>In Vitro</italic>. PLoS One 2013;8:e62953.
[14] Guilak F, Cohen DM, Estes BT, Gimble JM, Liedtke W, Chen CS. Control of Stem Cell Fate by Physical Interactions with the Extracellular Matrix. Cell Stem Cell 2009;5:17-26.
[15] Dalby MJ, Gadegaard N, Oreffo ROC. Harnessing nanotopography and integrin-matrix interactions to influence stem cell fate. Nat Mater 2014;13:558-69.

[16] Discher DE, Mooney DJ, Zandstra PW. Growth Factors, Matrices, and Forces Combine and Control Stem Cells. Science 2009;324:1673-7.
[17] Hickman GJ, Boocock DJ, Pockley AG, Perry CC. The Importance and Clinical Relevance of Surfaces in Tissue Culture. ACS Biomater-Sci Eng 2016;2:152-64.
[18] Edgar D, Kenny S, Almond S, Murray P. Topography, stem cell behaviour, and organogenesis. Pediatr Surg Int 2004;20:737-40.
[19] Li HQ, Wen F, Chen HZ, Pal M, Lai YK, Zhao AZ, Tan LP. Micropatterning Extracellular Matrix Proteins on Electrospun Fibrous Substrate Promote Human Mesenchymal Stem Cell Differentiation Toward Neurogenic Lineage. Acs Applied Materials & Interfaces 2016;8:563-73.
[20] Kim J, Staunton JR, Tanner K. Independent Control of Topography for 3D Patterning of the ECM Microenvironment. Adv Mater 2016;28:132-+.
[21] Zhang L, Webster TJ. Nanotechnology and nanomaterials: Promises for improved tissue regeneration. Nano Today 2009;4:66-80.
[22] Goreham RV, Mierczynska A, Smith LE, Sedev R, Vasilev K. Small surface nanotopography encourages fibroblast and osteoblast cell adhesion. RSC Advances 2013;3:10309-17.
[23] Ross AM, Jiang Z, Bastmeyer M, Lahann J. Physical Aspects of Cell Culture Substrates: Topography, Roughness, and Elasticity. Small 2012;8:336-55.
[24] Bettinger CJ, Langer R, Borenstein JT. Engineering Substrate Topography at the Micro- and Nanoscale to Control Cell Function. Angew Chem Int Ed 2009;48:5406-15.
[25] McNamara LE, McMurray RJ, Biggs MJP, Kantawong F, Oreffo ROC, Dalby MJ. Nanotopographical Control of Stem Cell Differentiation. Journal of Tissue Engineering 2010;1.
[26] Dalby MJ, Gadegaard N, Tare R, Andar A, Riehle MO, Herzyk P, Wilkinson CD, Oreffo RO. The control of human mesenchymal cell differentiation using nanoscale symmetry and disorder. Nature materials 2007;6:997-1003.
[27] Teo BKK, Wong ST, Lim CK, Kung TYS, Yap CH, Ramagopal Y, Romer LH, Yim EKF. Nanotopography Modulates Mechanotransduction of Stem Cells and Induces Differentiation through Focal Adhesion Kinase. ACS Nano 2013;7:4785-98.
[28] Harding F, Goreham R, Short R, Vasilev K, Voelcker NH. Surface Bound Amine Functional Group Density Influences Embryonic Stem Cell Maintenance. Advanced Healthcare Materials 2013;2:585-90.
[29] Wells N, Baxter MA, Turnbull JE, Murray P, Edgar D, Parry KL, Steele DA, Short RD. The geometric control of E14 and R1 mouse embryonic stem cell pluripotency by plasma polymer surface chemical gradients. Biomaterials 2009;30:1066-70.
[30] Murray P, Prewitz M, Hopp I, Wells N, Zhang H, Cooper A, Parry KL, Short R, Antoine DJ, Edgar D. The self-renewal of mouse embryonic stem cells is regulated by cell–substratum adhesion and cell spreading. The International Journal of Biochemistry & Cell Biology 2013;45:2698-705.
[31] Borghi FF, Rider AE, Kumar S, Han ZJ, Haylock D, Ostrikov K. Emerging Stem Cell Controls: Nanomaterials and Plasma Effects. Journal of Nanomaterials 2013;2013:15.
[32] M. MacGregor-Ramiasa, Vasilev K. Plasma polymer deposition: a versatile tool for stem cell research. In: Tiwari A, editor. Advanced surface for stem cell research. Wiley2016.
[33] Chu PK, Chen JY, Wang LP, Huang N. Plasma-surface modification of biomaterials. Materials Science and Engineering: R: Reports 2002;36:143-206.
[34] Zhu T, Vasilev K, Kreiter M, Mittler S, Knoll W. Surface Modification of Citrate-Reduced Colloidal Gold Nanoparticles with 2-Mercaptosuccinic Acid. Langmuir 2003;19:8.

584 [35] Turkevich J, Stevenson PC, Hillier J. A Study of the Nucleation and Growth Processes in
585 the Synthesis of Colloidal Gold. Discussions of the Faraday Society 1951;11:23.
586 [36] Griesser HJ. Small scale reactor for plasma processing of moving substrate web. Vacuum
587 1989;39:485-8.
588 [37] Goreham RV, Mierczynska A, Pierce M, Short RD, Taheri S, Bachhuka A, Cavallaro A,
589 Smith LE, Vasilev K. A substrate independent approach for generation of surface gradients. Thin
590 Solid Films 2013;528:106-10.
591 [38] Shankland SJ, Pippin JW, Reiser J, Mundel P. Podocytes in culture: past, present, and
592 future. Kidney Int 2007;72:26-36.
593 [39] Schneider CA, Rasband WS, Eliceiri KW. NIH Image to ImageJ: 25 years of image
594 analysis. Nat Meth 2012;9:671-5.
595 [40] Mierczynska A, Michelmore A, Tripathi A, Goreham RV, Sedev R, Vasilev K. pH-tunable
596 gradients of wettability and surface potential. Soft Matter 2012;8:8399-404.
597 [41] Delalat B, Goreham RV, Vasilev K, Harding FJ, Voelcker NH. Subtle Changes in Surface
598 Chemistry Affect Embryoid Body Cell Differentiation: Lessons Learnt from Surface-Bound
599 Amine Density Gradients. Tissue Engineering Part A 2013;20:1715-25.
600 [42] Liu X, Shi S, Feng Q, Bachhuka A, He W, Huang Q, Zhang R, Yang X, Vasilev K. Surface
601 Chemical Gradient Affects the Differentiation of Human Adipose-Derived Stem Cells via
602 ERK1/2 Signaling Pathway. ACS Applied Materials & Interfaces 2015;7:18473-82.
603 [43] Michelmore A, Martinek P, Sah V, Short RD, Vasilev K. Surface Morphology in the Early
604 Stages of Plasma Polymer Film Growth from Amine-Containing Monomers. Plasma Processes
605 and Polymers 2011;8:367-72.
606 [44] Saleem MA, O'Hare MJ, Reiser J, Coward RJ, Inward CD, Farren T, Xing CY, Ni L,
607 Mathieson PW, Mundel P. A conditionally immortalized human podocyte cell line
608 demonstrating nephrin and podocin expression. J Am Soc Nephrol 2002;13:630-8.
609 [45] Mattei G, Ferretti C, Tirella A, Ahluwalia A, Mattioli-Belmonte M. Decoupling the role of
610 stiffness from other hydroxyapatite signalling cues in periosteal derived stem cell differentiation.
611 Sci Rep 2015;5:10778.
612 [46] Ramiasa-MacGregor M, Mierczynska A, Sedev R, Vasilev K. Tuning and predicting the
613 wetting of nanoengineered material surface. Nanoscale 2016;8:4635-42.
614 [47] Vasilev K. Nanoengineered plasma polymer films for biomaterial applications. Plasma
615 Chem Plasma Process 2013:1-14.
616 [48] Goreham RV, Short RD, Vasilev K. Method for the Generation of Surface-Bound
617 Nanoparticle Density Gradients. The Journal of Physical Chemistry C 2011;115:3429-33.
618 [49] Bosman FT, Stamenkovic I. Functional structure and composition of the extracellular
619 matrix. J Pathol 2003;200:423-8.
620 [50] Bozec L, Horton MA. Skeletal tissues as nanomaterials. J Mater Sci Mater Med
621 2006;17:1043-8.
622 [51] Variola F, Brunski JB, Orsini G, Tambasco de Oliveira P, Wazen R, Nanci A. Nanoscale
623 surface modifications of medically relevant metals: state-of-the art and perspectives. Nanoscale
624 2011;3:335-53.
625 [52] Erickson HP. Size and Shape of Protein Molecules at the Nanometer Level Determined by
626 Sedimentation, Gel Filtration, and Electron Microscopy. Biol Proced Online 2009;11:32-51.
627 [53] Dulgar-Tulloch AJ, Bizios R, Siegel RW. Human mesenchymal stem cell adhesion and
628 proliferation in response to ceramic chemistry and nanoscale topography. Journal of Biomedical
629 Materials Research Part A 2009;90A:586-94.

630 [54] Rebollar E, Frischauf I, Olbrich M, Peterbauer T, Hering S, Preiner J, Hinterdorfer P,
631 Romanin C, Heitz J. Proliferation of aligned mammalian cells on laser-nanostructured
632 polystyrene. Biomaterials 2008;29:1796-806.
633 [55] Liu X, Feng Q, Bachhuka A, Vasilev K. Surface chemical functionalities affect the behavior
634 of human adipose-derived stem cells in vitro. Appl Surf Sci 2013;270:473-9.
635 [56] Kreidberg JA. Podocyte Differentiation and Glomerulogenesis. J Am Soc Nephrol
636 2003;14:806-14.
637 [57] Cha C, Liechty WB, Khademhosseini A, Peppas NA. Designing Biomaterials To Direct
638 Stem Cell Fate. ACS Nano 2012;6:9353-8.
639 [58] Yim EKF, Pang SW, Leong KW. Synthetic nanostructures inducing differentiation of
640 human mesenchymal stem cells into neuronal lineage. Exp Cell Res 2007;313:1820-9.
641 [59] Migliorini E, Grenci G, Ban J, Pozzato A, Tormen M, Lazzarino M, Torre V, Ruaro ME.
642 Acceleration of neuronal precursors differentiation induced by substrate nanotopography.
643 Biotechnol Bioeng 2011;108:2736-46.
644 [60] Xie J, Willerth SM, Li X, Macewan MR, Rader A, Sakiyama-Elbert SE, Xia Y. The
645 differentiation of embryonic stem cells seeded on electrospun nanofibers into neural lineages.
646 Biomaterials 2009;30:354-62.
647 [61] Dang JM, Leong KW. Myogenic Induction of Aligned Mesenchymal Stem Cell Sheets by
648 Culture on Thermally Responsive Electrospun Nanofibers. Advanced materials (Deerfield
649 Beach, Fla) 2007;19:2775-9.
650 [62] Grinstein M, Yelin R, Herzlinger D, Schultheiss TM. Generation of the podocyte and
651 tubular components of an amniote kidney: timing of specification and a role for Wnt signaling.
652 Development 2013;140:4565-73.

653

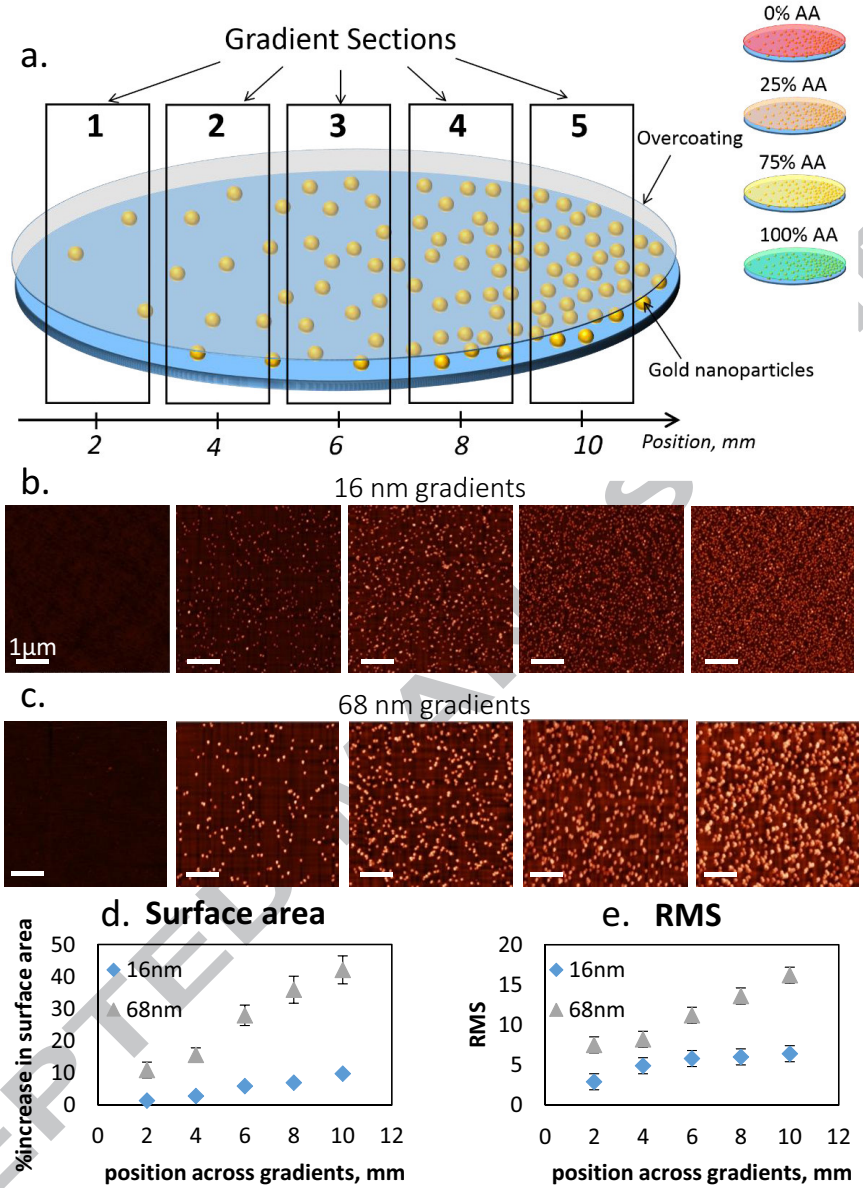

a.

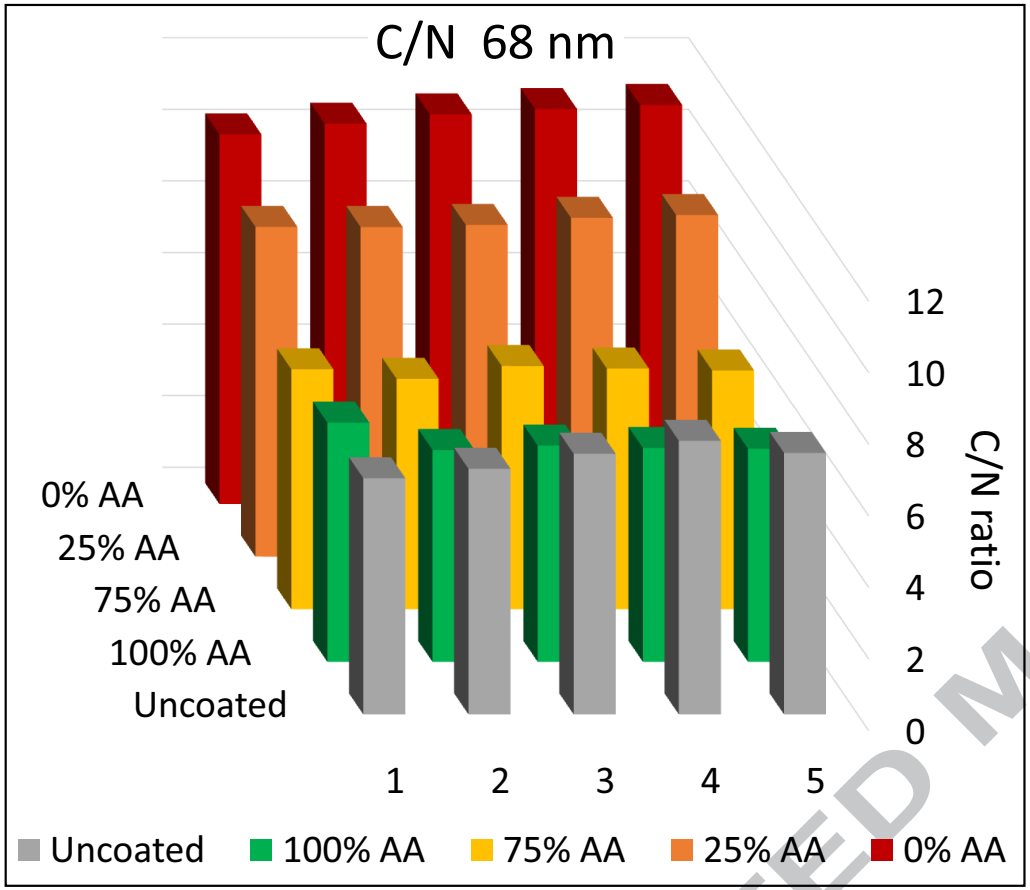

b.

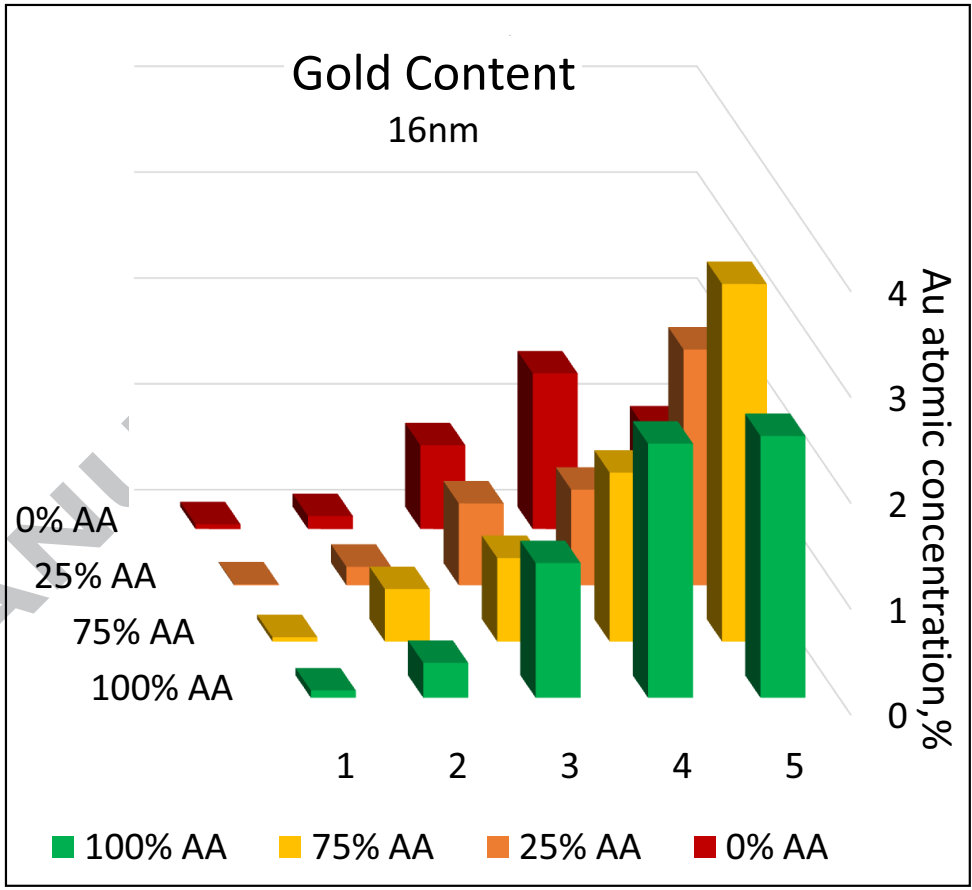

Figure(s)

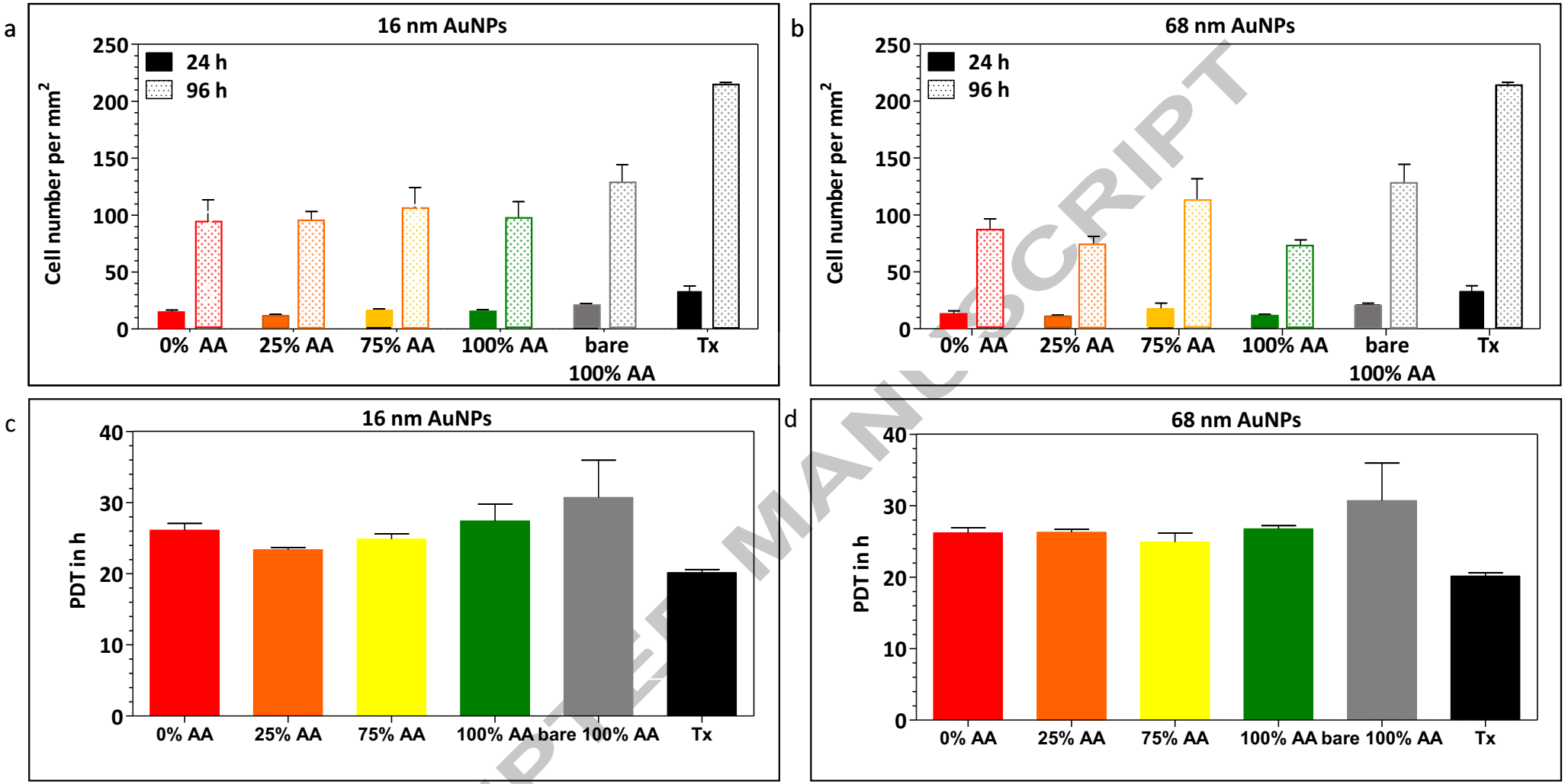

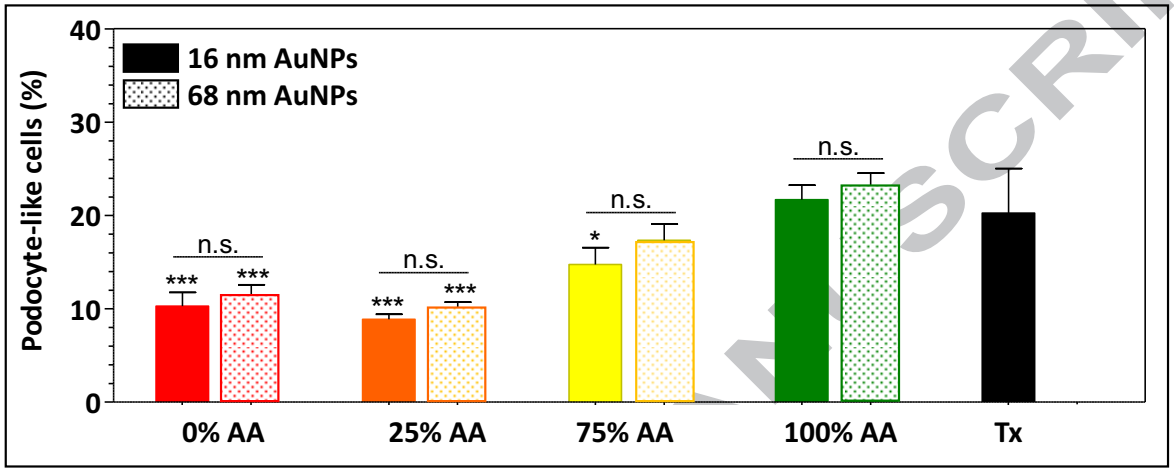

Figure(s)

a.

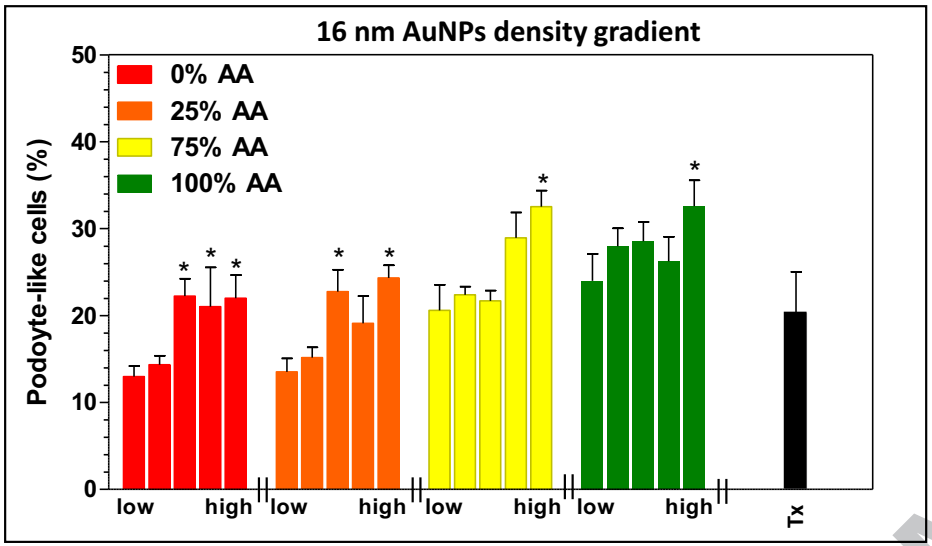

b.

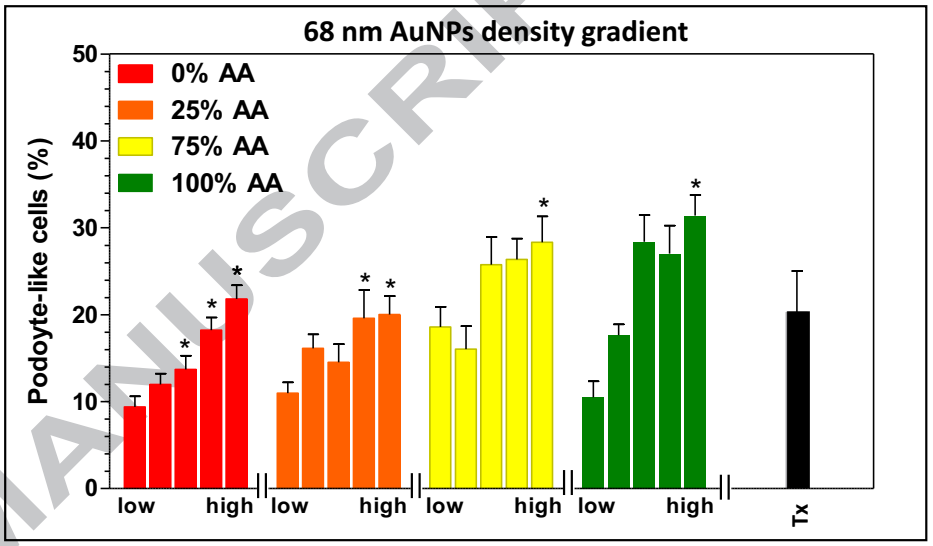

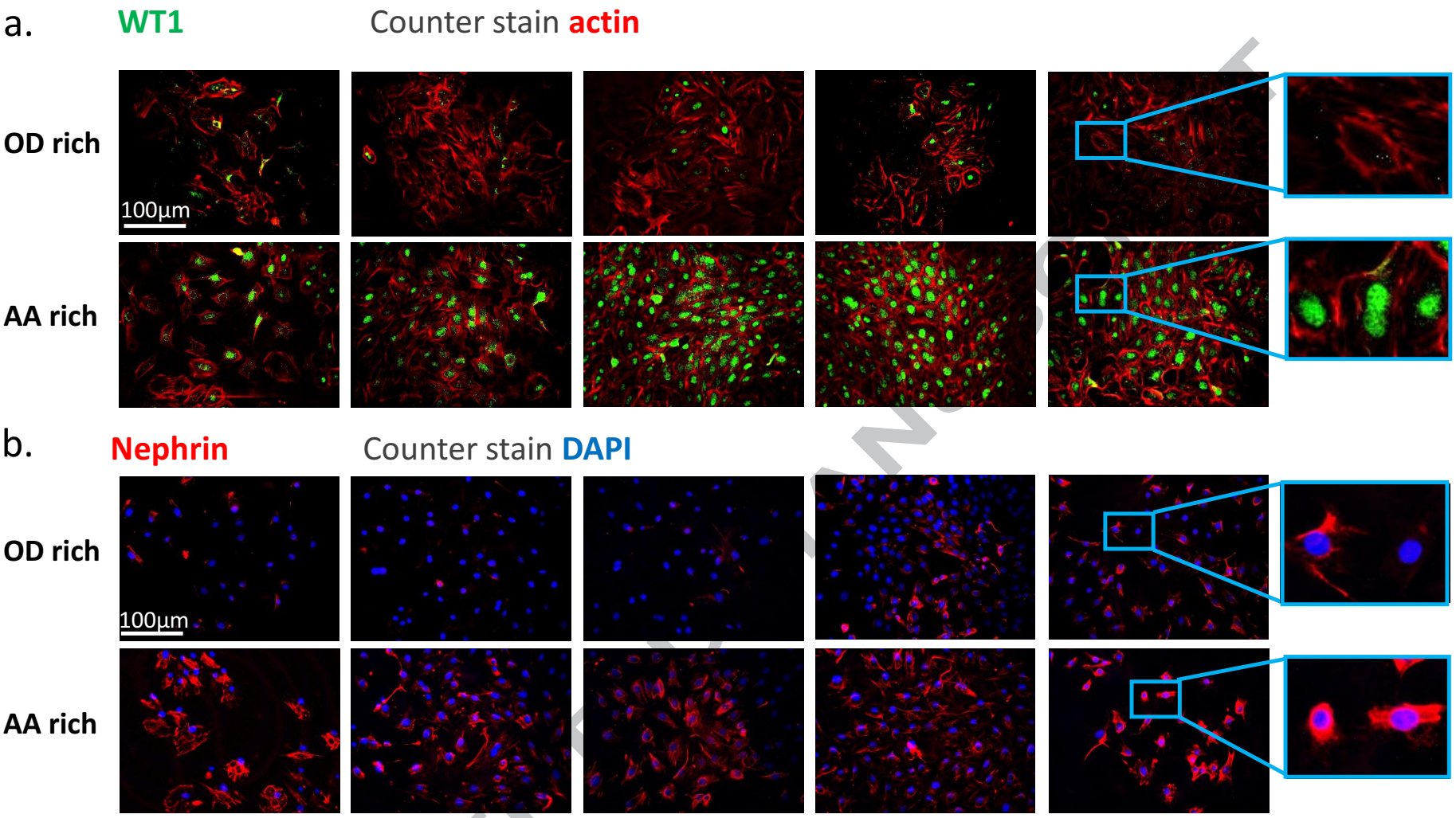

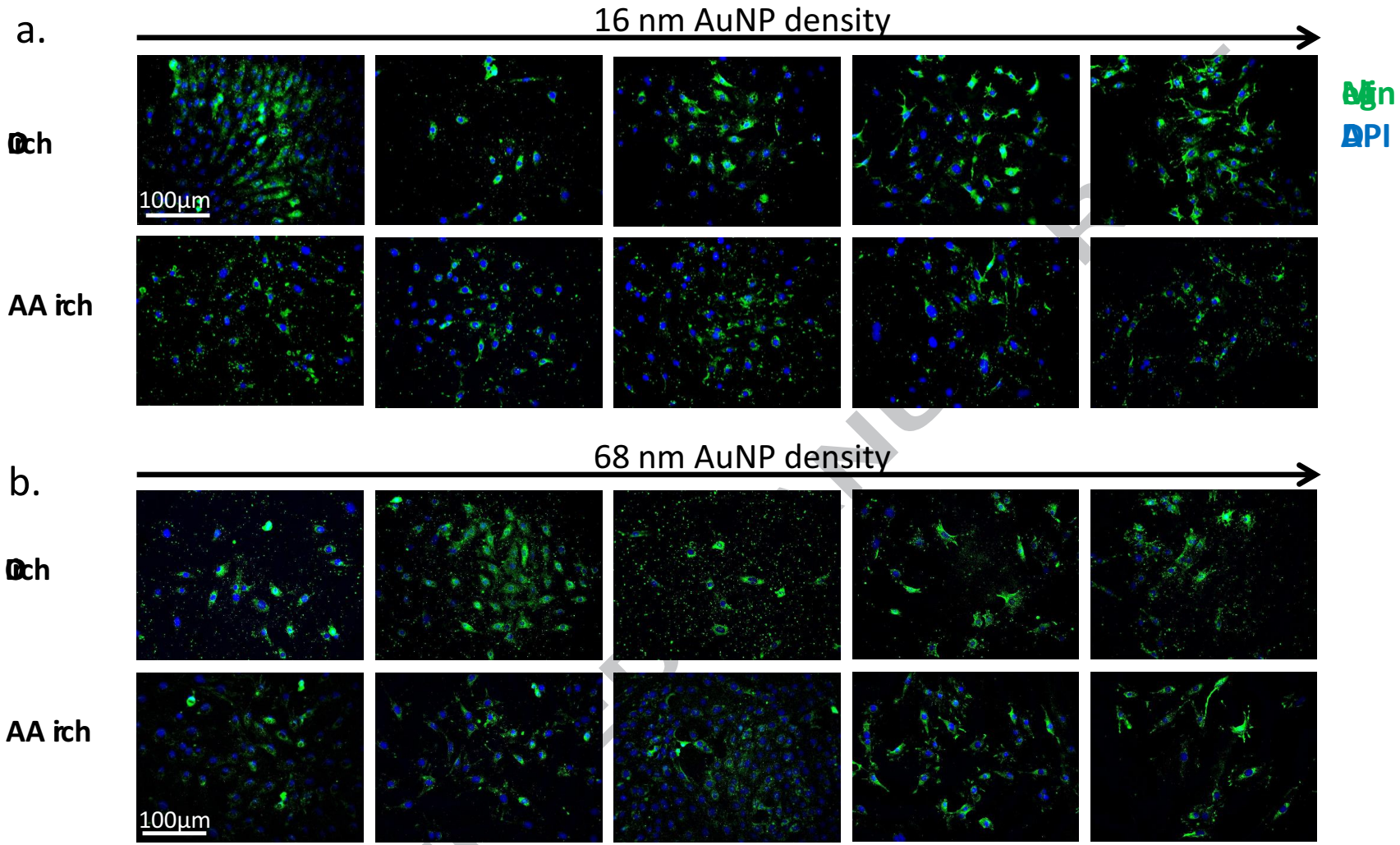

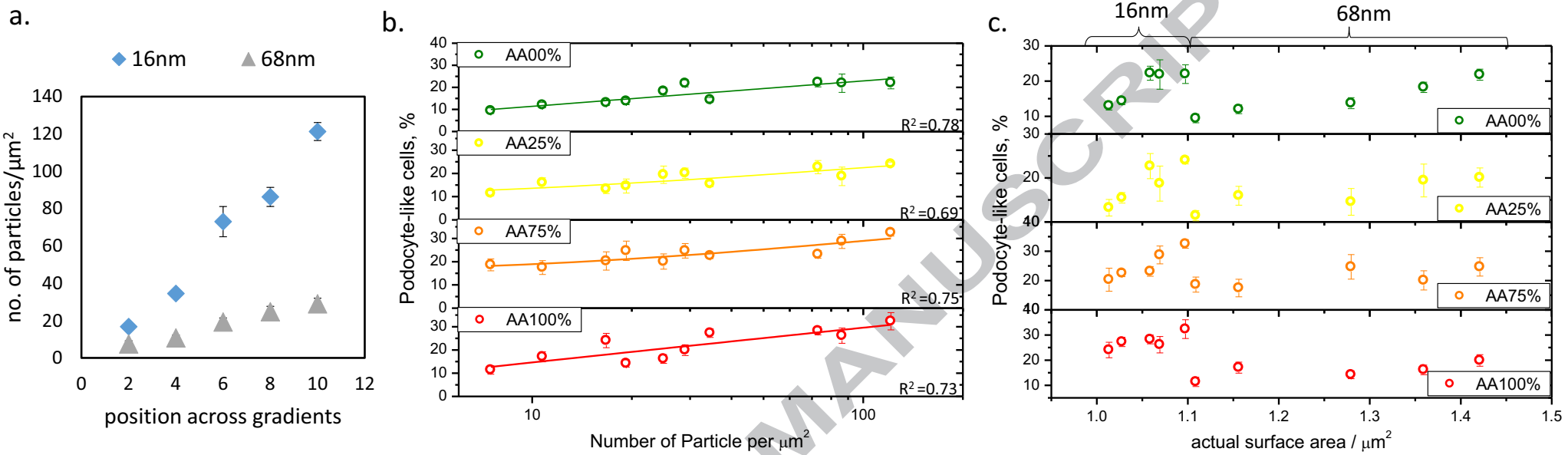

Surface Nanotopography guides Kidney-derived Stem Cells Differentiation into Podocytes

Melanie MacGregor-Ramiasa[a]‡, *Isabel Hopp*[b]‡, *Akash Bachhuka*[a], *Patricia Murray*[b]* *and Krasimir Vasilev*[c]*

SIGNIFICANCE STATEMENT

Adult kidney-derived *stem cells* have been identified as a promising way to regenerate damaged nephrons. Artificial growth platforms capable to guide the stem cells differentiation into useful cell lineages are needed to expand regenerative cell therapies for chronic kidney diseases. Chemically homogeneous growth substrates endowed with nanotopography gradients were generated via plasma assisted methods in order to investigate the effect of physical cues on the proliferation and differentiation of kidney-derived stem cells. For the first time it is shown that the surface density of the nano-structures had a greater impact on fate of the stem cells than their size. Careful design of the growth substrate nanotopography may help directing the differentiation into either podocytes or proximal tubule cells.